Visual Abstract

Review of current developments on high strength pipeline steels for HIC inducing service

Ehsan Entezari, Jorge Luis González-Velázquez, Diego Rivas López, Manuel Alejandro Beltrán Zúñiga
Department of Metallurgy and Materials, Escuela Superior de Ingeniería Química e Industrias Extractivas, Instituto Politécnico Nacional, Mexico
ehsan.entezari2014@gmail.com, https://orcid.org/0000-0003-3379-1761
jlgonzalezv@ipn.mx, https://orcid.org/0000-0001-6914-4449
drivasl@ipn.mx, https://orcid.org/ 0000-0003-4591-719X
mabz_2205@hotmail.com, https://orcid.org/0000-0003-4201-9896

Jerzy A. Szpunar
Department of Mechanical Engineering, University of Saskatchewan, Canada
jerzy.szpunar@usask.ca, https://orcid.org/0000-0002-1291-8375

ABSTRACT. Nowadays, an increasing number of oil and gas transmission pipes are constructed with high-strength low alloy steels (HSLA; nonetheless, many of these pipelines suffer from different types of hydrogen damage, including hydrogen-induced cracking (HIC). Many studies are being done to investigate the role of key metallurgical and processing factors to limit the negative effects of HIC in HSLA steel pipes.
The thermomechanical control process (TMCP) is a microstructural control technique that avoids the conventional heat treatment after hot rolling and attempts to obtain the desired mechanical properties during the forming process. Recent research has shown that TMCP provides high HIC resistance without adding high amounts of alloying elements or applying expensive heat treatments. However, there is an incipient knowledge on predicting HIC behavior, both in susceptibility and kinetics, in HSLA steel pipe when it is exposed to hydrogen charging service conditions.
This paper presents a review of the current developments of HSLA and TMCP of pipeline steels, as well as the phenomenological and empirical models proposed to predict the kinetics of HIC as a function of key parameters such as heat treatments and microstructures, especially nature and spatial distribution of non-metallic inclusions and the hydrogen permeation rate and the mechanical and fracture mechanics properties.

KEYWORDS. High strength pipeline steels; Hydrogen-induced cracking; Thermomechanical controlled process; HIC growth rate models.

OPEN ACCESS

Citation: Entezari, E., González-Velázquez, J.L., Rivas López, D., Beltrán Zúñiga, M.A., Szpunar, J.A., Review of current developments on high strength pipeline steels for HIC inducing service, Frattura ed Integrità Strutturale, 61 (2022) 20-45.

Received: 28.12.2022
Accepted: 03.04.2022
Online first: 14.04.2022
Published: 01.07.2022

INTRODUCTION

The growing demand for high-strength steels with good HIC resistance for oil and gas transmission pipelines has led to research on optimizing the composition and thermomechanical processing routes.

The alloy design of new generations of pipeline steels is mainly focused on manufacturing micro-alloyed steels. This is because the microstructural features of them allow both improving the mechanical properties and weldability, yet at lower production costs since they eliminate the use of expensive alloying elements and heat treatment [1, 2]. Nowadays, thermodynamics models such as MUCG83, JMatPro, and Thermo-Calc will provide the opportunity to design pipeline steels with new chemical compositions [3-5]. Salt bath heat treatment (quenching-partitioning process) and thermomechanical control process (TMCP) are two main processing routes for producing pipeline steels [6-8]. Zhao and al. [9] suggested that the TMCP provides better microstructural control and shortens processing routes. The balanced combination of finish rolling temperature (FRT) and finish cooling temperature (FCT) and optimizing the cooling rate during TMCP led to a microstructural refinement that enhances the mechanical properties combination, as shown by Jiang and al. [10]. From a metallurgical point of view, pipeline steels with bainitic and martensitic microstructures have been employed in the manufacturing of recent oil and gas pipelines in applications that demand an excellent combination of high strength and toughness with small wall thickness, such as high pressure and long-distance transportation systems [11, 12].

With the increasing acidity of crude oils and natural gas, the hydrocarbon transportation systems are increasingly experiencing hydrogen-induced cracking (HIC), stress-oriented hydrogen-induced cracking (SOHIC), stress corrosion cracking (SCC), and sulfide stress cracking (SSC). Among these damage mechanisms, HIC is considered one of the most important threats to structural integrity, mainly because of its high frequency of occurrence [13].

The standards NACE TMO-284, NACE TMO-177, and NACE TMO-103 were published in the 1980s as laboratory test methods to evaluate the hydrogen cracking resistance of the pipeline steels [14-17]; however, they were basically screening methods for material selection, but do not provide data to predict the HIC remaining strength and remaining life of pipeline steels in hydrogen charging environments.

Arafin and al. [18] and Moon and al. [19] showed granular bainite and tempered martensite have excellent resistance against HIC cracking. Furthermore, it has been demonstrated that non-metallic inclusions (NMI) act as irreversible hydrogen trapping sites where the accumulation of hydrogen atoms at the interface of inclusions and the steel matrix promotes HIC [20]. Many researchers showed that elements such as manganese (less than 2 Wt. %), chromium (Less than 0.3 Wt. %), molybdenum (Less than 0.4 Wt. %), phosphorus (Less than 0.008 Wt. %), and copper (above 0.2 Wt.%) along with niobium, vanadium, titanium, and calcium enhance the HIC resistance of pipeline steels. It is suggested that these alloying elements may control the phase transformation temperature and the rate of hydrogen diffusion, as well as controlling NMI morphology, providing a path to develop high HIC resistance steels for pipeline manufacturing [21-26].

Usually, pH and hydrogen partial pressure (pH_2S) have been regarded as key environmental factors to determine the severity of HIC damage. In general, it has been observed that the reduction of pH and increment of pH_2S increase the hydrogen flux, leading to a higher HIC susceptibility [27]. Also, residual stress caused by inhomogeneous plastic deformation and incorrect welding processes is a well-known factor that increases the severity of HIC in sour oil and gas pipelines [27, 28].

Ongoing investigations indicate that the kinetics of HIC in oil and gas transmission pipes exposed to sour environments can be predicted by phenomenological, empirical, and numerical methods [29, 30]. These findings have encouraged the idea by combining the results of research-oriented to develop high strength steels that are resistant to HIC with the phenomenological and analytical methods to predict HIC kinetics that can lead to the development of FFS algorithms to assess HIC with reasonable accuracy.

The present review paper summarizes the processing routes to produce high-strength steel pipes and describes their metallurgical and mechanical characteristics, and also, it reviews the main parameters used in the kinetic modeling of HIC such as microstructures, especially nature and spatial distribution of non-metallic inclusions, and the hydrogen permeation rate, and mechanical and fracture mechanics properties.

STEEL PROCESSING

Alloy designing

In the modern pipeline industry, the need to reduce costs and time to design and produce improved steels that satisfy requirements of higher strength and defects tolerance has encouraged many researchers to use thermodynamic models such as MUCG83, JMatPro, and Thermo-Calc [3-5].

MUCG83 is a thermodynamic model developed by Bhadeshia [31] based on thermodynamic and kinetics of solid-state phase transformation in steels. The software uses the chemical composition as an input parameter, and the time-temperature-transformation (TTT) diagrams are the output data of the software.
The developments in the design of thermomechanical heat treatment schedules have led to a new multi-platform software known as JMatPro, which generates continuous cooling transformation (CCT) diagrams [32]. The advantage of this thermodynamic model is that only a few experimental data are required as input, and since it considers the effect of cooling rate, it can be applied to hot rolling and other processes that involve continuous cooling.
Another well-known method for optimizing the chemical composition of steels in alloy designing is using thermo-calc TCFE6 database software [33]. Many researchers used thermo-calc models to predict microstructural, mechanical properties, and continuous cooling transformations [34-36].
The chemical compositions of high-strength pipeline steels have been continuously modified in the last decades in order to improve strength, toughness, and weldability. Usually, the chemical composition of API-5XL steel grades contains < 0.1 Wt.% of carbon, < 0.6 Wt.% silicon, and up to 20 Wt.% manganese, with additions of less <0.6Wt.% of each of niobium, titanium, vanadium, and molybdenum [37].
The main role of the alloying elements used for improving the strength is through grain refinement and precipitate dispersion hardening. Alloying elements also affect the transformation temperature, which allows microstructural control during hot rolling operations. Tab. 1 illustrates the influence of alloying elements on improving the microstructural characteristics and mechanical properties of high strength pipeline steels without compromising weldability, especially [37-39]:

- Molybdenum (Mo), silicon (Si), nickel (Ni), and Nb + V: all contribute to increased steel strength.
- Ni+ Mo: affect microstructure refinement achieved by suppressing austenite recrystallization, as well as steel strengthening through precipitation hardening and hardenability enhancement.
- Ni+ B: improve hardenability synergistically.
- V+Mo+Nb: affect secondary hardening achieved by producing carbides, nitrides, and carbonitrides.
- Mo+Nb+Ti: more effective in improving the strength requirements obtained by finer ferrite grain size and precipitation hardening.

The new generations of high-strength pipeline steels are classified into different categories based on microalloying. X70 steel is micro-alloyed with niobium and vanadium with reduced carbon content to enhance the precipitate hardening and grain refinement [40]. X80 steel has further reduced carbon content for weldability improvement [41]. The addition of molybdenum, copper, and nickel enhances the strength and low-temperature toughness of X100 steel. As mentioned before, high-strength pipeline steels, such as grade X100, offer the possibility of constructing high-pressure service (≥ 15 Mpa) and high flow rate pipelines that allow reducing the transport and construction costs by 30 % compared with X70 and X80 pipeline steels [40, 42]. Recently X120 steel has been introduced for improving the transport efficiency of ultra-high-pressure service. This type of steel is micro-alloyed with nickel, chromium, molybdenum, niobium, titanium, and copper to enhance strength by grain refinement and fine dispersions of hard second phases such as bainite [41].

Heat treatment methods

Salt bath heat treatment is characterized by fast and homogeneous heating, controlled quenching, low surface oxidation, and improved decarburization, which is advantageous compared to traditional oil or water quenching media [43]. Tab. 2 shows the types of heat treatment applied in the fabrication of high-strength steels as a function of salt bath chemical composition and temperature [43].
Quenching- partitioning- tempering (Q-P-T) heat treatment is a combination of heat treatment processes listed in Tab. 2. It is used for manufacturing high-strength steel with an excellent combination of strength and toughness. The Q-P-T treatment starts with austenitization, followed by quenching in a salt bath at temperatures between martensite-start (M_S) and martensite-finish (M_f) temperature for a specified time and finally quenching in water. This treatment promotes the diffusion of carbon from the supersaturated martensite to the retained austenite and stable ferrite regions, producing a very fine dispersion of carbides, combined with interstitial solid solution hardening [44, 45].
Since salt bath heat treatment processes are time-consuming and are limited by the size of the molten salt bath, a thermomechanical controlled process (TMCP) is another option to produce high-strength pipeline steel [6,7]. Thermo-mechanical controlled processing (TMCP) is a technique for controlling the hot-deformation process in a rolling mill to improve the mechanical properties of steels. By minimizing or even eliminating heat treatment after hot-deformation, such processing saves energy in the steel manufacturing process, increasing productivity for high-grade steels. It usually necessitates a change in alloy design that allows for both a reduction in total alloying additions and improved weldability [39]. Further, the preheating temperature, non-recrystallization temperature (Tnr), finish cooling temperature (FCT), and

finish rolling temperature (FRT) are key temperature parameters used in this process [43]. Tab. 3 shows the combination of FCT, FRT, and cooling rate, typically used in TMCP [46-58].

Alloying elements	Strengthening	Hardenability	Grain refinement	Toughness properties	Suppressing recrystallization	Controlling Phase transformation	Controlling Phase transformation
C	●						
Mn	●		●	●		●	
Ni	●			●			●
V	●						
Si	●						
Ti	●	●	●				
Mo	●	●				●	
Nb			●		●		
B	●	●	●				
Ni + Mo	●	●			●		
Ni + B		●		●			
Nb + V	●						●
V + Mo + Nb	●	●					
Mo + Nb + Ti	●	●	●			●	

Table 1: Simplified illustration of alloying elements on microstructural and mechanical properties of high-strength pipeline steels.

Typically, TMCP includes three steps: reheating, rolling, and cooling. Strengthening microstructural factors such as grain size, precipitate size and spacing, solid solution, and dislocation hardening can be controlled by key temperature parameters during each step of TMCP [48, 59].
In the last decade, offshore structures have been constructed in colder regions and deeper water, demanding low thickness and high strength pipeline steels with improved toughness, weldability, and excellent HIC resistance. This has encouraged steel manufacturers to use processing routes such as TMCP to produce pipeline steels with the desired mechanical and in-service damage resistance properties [46, 60].

The metallurgical characteristics of TMCP steels

The new generation of API-5XL steels is classified into four categories based on microstructural control, as indicated in Tab. 4 [60-67].
The main strategy to fabricate API 5XL steels is to obtain fine microstructural features by controlling key temperature parameters such as Tnr, FCT, FRT during TMCP, which improves mechanical properties. Further, the interaction between chemical composition and controlled cooling rate is more effective in generating a microstructure with fine grain size (low angle boundaries) that inhibits dislocation movement, resulting in an ideal combination of strength and toughness at temperatures as low as -40 °C. As a result, the chemical elements mentioned in Tab. 1 can affect the cooling rate and subsequently control the grain size during the TMCP process [39].
Accelerated cooling, quenching and tempering, and the online heat treatment process are used for producing pipeline steels with bainite-martensite microstructure. Tempering reduces the brittleness of martensite and enhances the toughness of pipeline steels by producing fine dispersions of carbides [44]. The online heat treatment process is applied to produce high-strength low alloy steel plates with thickness up to 40 mm [39].

Heat treatment types	Heat treatment temperature range (°C)	Bath components	Composition (Wt.%)	Melting temperature (°C)	Operating temperature range (°C)
Austempering	200-400	KNO_3 $NaNO_2$	50-60 40-50	135	160-550
		$NaNO_3$ $NaNO_2$	50-60 40-50	145	150-500
		KNO_3 $NaNO_3$	50-60 40-50	225	250-600
Martempering	Above Ms	KNO_3	100	337	350-500
		$NaNO_3$	100	370	400-600
		KNO_3 $NaNO_2$	50-60 40-50	135	160-550
		$NaNO_3$ $NaNO_2$	50-60 40-50	145	150-500
		KNO_3 $NaNO_3$	50-60 40-50	225	250-600
Hardening	760-1260	NaCl KCl $BaCl_2$ $CaCl_2$	10-15 20-30 40-50 15-20	400	500-800
		$NaCO_3$ KCl	45-55 45-55	450	550-900
		$BaCl_2$ KCl2 NaCl	50 30 20	40	570-900
		$BaCl_2$ NaCl	70-96 4-30	600-800	700-1250
Quenching - partitioning	Quenching between M_s and M_f & partitioning above Ms	KOH NaOH	60-75 25-40	130-160	150-350

Table 2: Types of heat treatment applied for the manufacturing of high-strength steels with the chemical composition and melting temperature of salt baths.

API- 5XL Steel grades	Finish Rolling Temperature (°C)	Finish Cooling Temperature (°C)	Cooling rate (°°C/S)	Ref
X70	750-850	450-600	16-23	[45,46]
X80	810-890	500-550	20-40	[47-49]
X100	800-830	250-530	30-38	[50-53]
X120	800-840	300-450	33-35	[54-56]

Table 3: The overview of a balanced combination of main temperatures parameters in TMCP.

API- 5XL Steel grades	Steel manufacturing process	Microstructure	Microstructural features
X70	TMCP + QT	Bainite-Martensite multiphase steel: *B+M+F	*Slender bainitic sheaves along with martensite laths [61]. *Smaller prior austenite grain (PAG) and fine ferrite grains [62]. *Martensite laths [61]. *High volume fraction of filmy austenite [63, 64]. ¤ polygonal and granular ferrite act as the second phase in the bainite matrix [65].
X80	TMCP + AcC	Bainite dual-phase steel: ¤B+F	
	TMCP + AcC + HOP	Bainite-Martensite multiphase steel: *B+M+A	
X100	TMCP + AcC + HOP	Bainite dual-phase steel: ¤B-F	
X120	TMCP + AcC	Martensite dual-phase steel: M+F	Fine ferrite acts as the second phase in the martensite matrix [66].
		Tempered Lath Martensite: TLM	Martensite laths [67].

Table 4: Classification of the new generation of high-strength pipeline steels based on microstructural control.

Polygonal and granular ferrite, austenite, martensite laths, slender bainitic sheaves, smaller prior austenite grains, and fine ferrite grains are microstructural features that can be accomplished by controlling temperature parameters during TMCP [60-66]. Such microstructural features can be achieved based on the manufacturing process mentioned in Tab. 4 and positively influence the mechanical properties of pipeline steels, as shown in Fig. 1 and Tab. 5 [48, 50, 52, 57, 62- 69].

Microstructure and mechanical properties

Tab. 6 presents data about the relationship between microstructure and chemical compositions of pipeline steels and their influence on tensile properties [39, 41, 48, 50, 52, 57]. As shown in Tab. 6, API X120 steel is micro-alloyed with different chemical elements, and also the amount of carbon content is reduced [41].

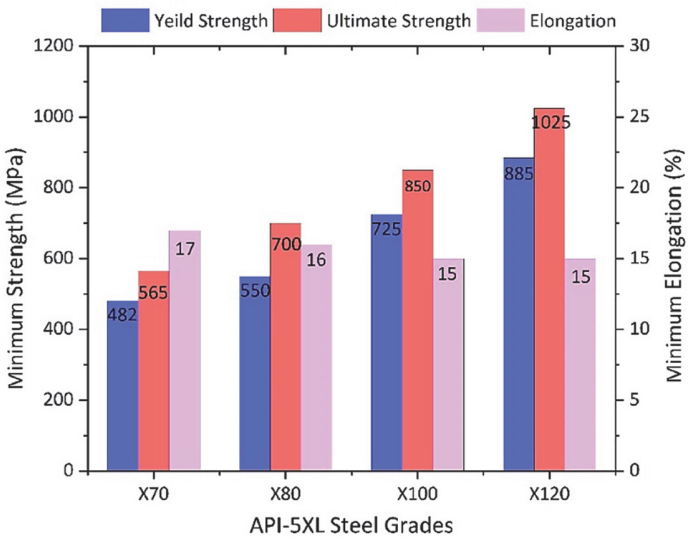

Figure 1: Minimum tensile properties of the new generation pipeline steels.

Microstructural Features	Effects	Ref
Fine ferrite grains	• Decrease in the slip length and slip reversibility. • Decrease in the slip deformation around the crack tip during crack propagation. • Decrease in dislocation pile-ups or an increase in the barriers of the crack propagation.	[65]
Smaller prior austenite grains		
Polygonal ferrite	• As a second phase in the bainite matrix significantly enhances both the yield strength and low-temperature toughness.	[68]
	• The enhancement of the fatigue limit of pipeline steels occurs.	[69]
Martensite laths	• The uniform distribution of dislocations and re-arrangement of stress concentration that occurs along the high angle grain boundaries. • Blockage of cleavage crack propagation by martensite lath boundaries acting as a barrier.	[64]
Filmy austenite	• Crack-tip blunting through the transformation retained austenite to the martensite and consumption a large amount of energy at crack tip (TRIP effect). • Decrease in the propagation rate and stress intensity factor of the main crack due to the compressive residual stress formation and propagation of the secondary crack resulting from the TRIP effect.	[69]
Bainitic sheaves	• Bainitic microstructures with a smaller width of the bainite laths have a higher stress intensity factor than the threshold value (K_{th}) for crack blunting.	[62, 64]

Table 5: The effect of positive microstructural features on microstructure- mechanical properties of pipeline steels.

API-5XL Steel grades Microstructure		X120		X100	X80		X70
		Tempered lath martensite (TLM)	Martensite dual phase steel (M + F)	Bainite dual phase steel (B + F)	Bainite Martensite multiphase steel (B + M + A)	Bainite dual phase steel (B + F)	Bainite Martensite multiphase steel (B + M + F)
Chemical composition (wt%)	C	0.075	0.070	0.080	0.080	0.080	0.075
	Mn	1.10	1.25	1.5	1.5	1.5	1.5
	Ni	1.25	1	-	-	-	0.6
	Si	0.5	0.5	0.25	0.25	0.25	0.3
	Mo	0.5	0.5	-	-	-	0.1
	Nb	0.07	0.04	0.04	0.04	0.04	0.06
	V	0.09	0.06	-	-	-	0.05
	Ti	0.03	0.03	-	-	-	0.04
σ_{yUTS} (MPa)		980	780	720	550	550	480
σ_{UTS} (MPa)		110	1000	850	680	680	620
El%		15	13	20	25	20	22

Table 6: The relationship between microstructures and chemical compositions and effects on tensile properties.

HYDROGEN INDUCED CRACKING (HIC)

HIC testing methods

When high-strength pipeline steels are exposed to hydrogen charging environments, such as sour environments, it is necessary to test HIC susceptibility.

The standard test method NACE TMO-284 evaluates the susceptibility to HIC by determining three parameters; crack length ratio (CLR), crack thickness ratio (CTR), and crack sensitivity ratio (CSR). In this testing method, unstressed specimens with dimensions 100 × 20 mm are exposed to synthetic seawater with pH=5 and purging H_2S gas or an H_2S/CO_2 mixture at room temperature for 96 hours. Fig. 2 illustrates the NACE TMO-284 test setup [14]. The acceptance criteria are CLR ≤15 %, CTR ≤ 5 %, and CSR ≤ 2%, according to the NACE MR 0175/ ISO 15156 [70]. A higher value of CSR indicates a higher susceptibility to HIC, whereas a higher value of CTR indicates more stepwise cracking, which makes HIC more severe from the mechanical point of view, according to the API 579-1/ASME FFS-1 standard. CTR also is related to microstructural banding or NMI content [70].

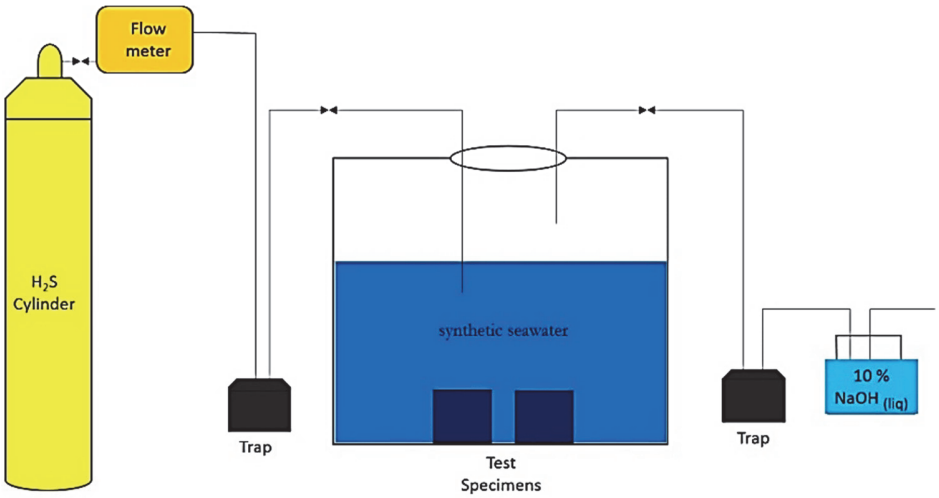

Figure 2: Schematic diagram of the NACE TMO-284 test.

The NACE TMO 177 is a testing method aimed to evaluate stress-orientated hydrogen-induced cracking (SOHIC) resistance in a sour environment [15]. In this testing method, hydraulic loading is applied for a fully machined specimen with dimensions 6.35 mm diameter, 25.4 mm gauge length, and 15-20 mm shoulder radius. Loading is controlled by constant load devices to limit load relaxation in the duration of testing. The test is conducted at 30 %, 50 %, and 90 % of the yield strength, as established in the NACE TMO103 standard test method. Accordingly, specimens that do not crack at 50 % yield have suitable resistance to SOHIC [15].

Additionally, in normal HIC, the cracks form groups of individual cracks aligned nearly parallel to the plate wall, but SOHIC occurs when HIC cracks combine with radial oriented cracks and merge to the surface, as shown in Fig. 3. Tensile or residual stress is required to produce SOHIC [15].

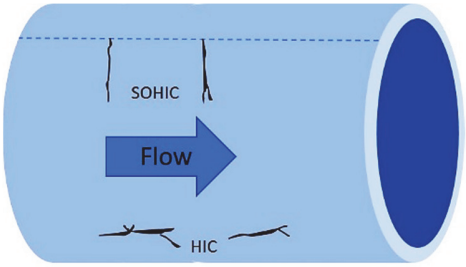

Figure 3: Schematic illustration of the morphology of hydrogen-induced cracking (HIC) and stress-oriented hydrogen-induced cracking (SOHIC) in the pipeline.

An alternative testing method to evaluate the resistance to SOHIC is four points bent double beam. In this testing method, a steel sample, containing a notch with 2 mm depth and 0.13 mm radius, are bolted back to back across a pair of rollers and thereby placed into 4 points bending and exposed to the hydrogen charging environment for 168 hours, as depicted in Fig. 4 [16].

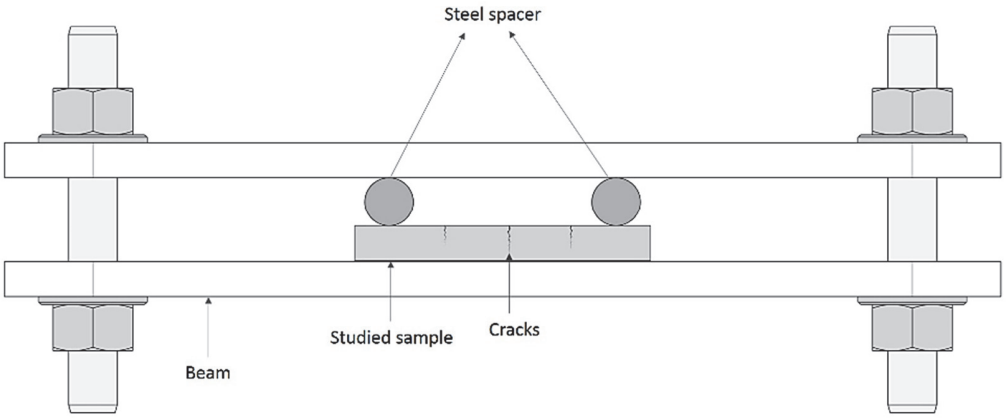

Figure 4: Full-size double-beam test specimen design.

An experimental method to artificially induce HIC is cathodic charging, which consists of an electrochemical cell where the test plate is connected as a cathode, and a piece of platinum is known as an anode. By applying a predetermined direct current and voltage, the hydrogen generated by the cathodic reaction is absorbed by the test specimen due to the poisoning effect of the electrolyte, specially formulated for that purpose [17], as shown in Fig. 5. Since the purpose of this test is to induce and observe the formation and growth of HIC cracks, therefore, the concentration and fugacity of hydrogen are not determined. The typical testing conditions of cathodic hydrogen charging are shown in Tab. 7 [18]. These conditions are empirical and have been demonstrated to be capable of inducing detectable HIC in the matter of several hours, which is very convenient for experimental purposes. During the test, specimens are examined from the unexposed face by straight beam ultrasonics to generate a C-scan map of the hydrogen-induced cracks. This test can be used to determine the HIC susceptibility by the NACE TM 284 criteria, but its greatest advantage is that it allows experimentally observing the HIC kinetics [17].

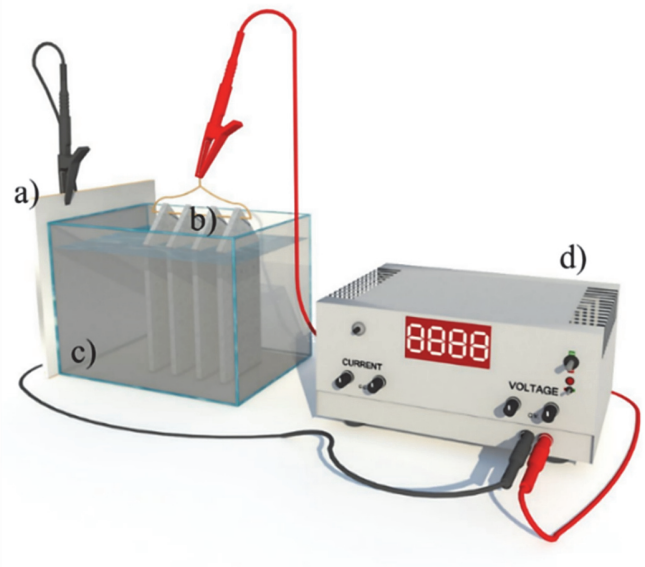

Figure 5: Schematic of the cathodic hydrogen charging experimental setup. a) test plate, b) anode (Pt), c) electrolyte solution with poison, d) DC power source.

Test parameter	Optimized condition
Current density	15-20 mA/Cm^2
Test duration	Variable
Electrolyte	H_2SO_4 solution with an addition of 20 mg/L As_2O_3
The total volume of electrolyte	750 ml
Argon gas purge	25 Cm^3/min
Testing temperature	Ambient
Testing pressure	Ambient

Table 7: Optimal testing condition of cathodic hydrogen charging.

Microstructure	Effect on HIC	Ref
Ferrite-pearlite dual phase F+P	• The ferrite-pearlite boundaries. are preferred paths for hydrogen crack propagations. • The intergranular fracture occurs along ferrite-perlite boundaries, and transgranular fracture occurs on slip plane occurs along slip planes.	[27]
	• The cementite lamellae has a lower hydrogen diffusivity than the spheroidal cementite. • High dislocation densities and large grain boundary areas increase hydrogen diffusivity. • Acicular ferrite delays HIC due to dispersed carbonitride precipitates and high-density of tangled dislocations.	[72]
	• High ferrite grain boundary areas per unit volume provides an efficient diffusion path for hydrogen transport, thus increasing the hydrogen concentration and the probability of HIC.	[73]
Martensite dual phase M+F / M+A	• Martensite-ferrite bands are efficient hydrogen trapping sites.	[27]
	• Propagation of HIC cracks along lath martensite is more likely because the lath martensite is inherently brittle due to its high dislocation density and high residual stresses. • The diffusion of hydrogen atoms significantly reduces the critical micro-strain for decohesion of ferrite-martensite plates, thus increasing the susceptibility to HIC. • HIC cracks initiate in martensite islands and propagate into ferrite areas.	[74]
	• Phase segregation regions in martensite-austenite microstructure are preferable sites for HIC.	[75]
Bainite dual phase GB + AF	• Granular bainite (GB) regions have are more resistance to HIC than the ferrite-pearlite regions. • High HIC resistance is due to the excellent resistance of ferrite against HIC.	[76]
	• Bainitic steel with lath morphology has low HIC resistance. • The high-volume fraction of bainitic laths leads to faster diffusion of hydrogen atoms, and a higher concentration of sub-surface hydrogen traps, consequently increase in the susceptibility to HIC.	[76]
Bainite-Martensite multiphase B-M-A / B-M-F	• Bainite-martensite multiphase steels have better resistance to HIC than the martensite dual-phase steels. • Bainite-martensite multiphase steel and ferrite-granular bainite perform similarly for HIC.	[77]
Tempered martensite	• Tempered martensite reduces hydrogen damage susceptibility by reducing the dislocations density and stored energy of martensite. • Nano-particles in tempered martensite decrease the mobility of hydrogen atoms and hydrogen concentration and thus reducing HIC susceptibility.	[78]
	• The quenching and tempering improve HIC resistance.	[79]

Table 8: Qualitative effects of steel microstructure on HIC resistance and susceptibility.

FACTORS OF IMPORTANCE FOR HIC CONTROL

Microstructure

The metallographic microstructure of the steel differently affects hydrogen diffusion rates and hydrogen atom trapping, thus influencing HIC. Tab. 8 shows the qualitative influence of microstructural features of API-5XL steels on HIC resistance or susceptibility [27, 72-79].

One of the most important microstructural features that affect HIC susceptibility is NMI. NMI is considered as the main hydrogen trap site to initiate HIC. NMI in pipeline steels typically are aluminum, silicon, magnesium, titanium oxides, and manganese sulfides [20, 27]. There are contradictions about the effect of NMI on HIC. Liu and al. [80] found that hydrogen cracking does not occur at SiO_2 precipitates; however, Xue and al. [81] observed HIC cracks initiate at SiO_2. Xue and al. [81] found that crack initiation did not occur at MnS inclusions in an API 5L X80 pipeline steel, even though it has been widely documented that HIC cracks initiate at elongated MnS inclusions [20, 27, 29]. In general, it is observed that multiple factors play a role in the effect of NMI on HIC in pipeline steels, such as morphology and size, the spatial distribution of NMI, elastic properties of the NMI and the matrix, and the crystallographic relationship between NMI and the matrix.

In the case of NMI morphology, Rahman and al. [82, 83] found that steel plates containing spinal and rectangular NMI are more susceptible to hydrogen cracking than globular NMI, assuming that globular NMI does not create regions with high-stress concentrations and they are not sufficiently brittle to initiate cracks.

However, the most important factor of NMI that affects HIC susceptibility is the inclusion size. The length of HIC cracks directly correlates with the length of NMI. Large NMI is prone to trap large quantities of hydrogen atoms and thus initiate hydrogen cracking [84]. Qin and al. [85] showed that the critical HIC cracks nucleation size with MnS and TiC inclusions is 10 μm and 335 nm, respectively.

The spatial distribution of NMI is another critical factor for HIC initiation. Rahman and al. [82] proposed a mathematical model that indicates that larger inclusion sizes and shorter distances among NMI reduce the plane strain fracture toughness at the interface of NMI, according to Eqn. (1).

$$K_{IC} = B\left[\wedge_1 \rho_1 \left(\frac{2a_1}{L}\right)^{\frac{n}{1+n}} + \wedge_2 \rho_2 \left(\frac{2a_2}{L}\right)^{\frac{n}{1+n}} + \wedge_3 \rho_3 \left(\frac{2a_3}{L}\right)^{\frac{n}{1+n}}\right]^{-1/2} \quad (1)$$

where $\wedge_i$, ρ_i, and a_i with i = 1, 2, and 3, represents the probability of cracking initiation at the interface of NMI, the density of NMI, and the average size of the NMI, respectively (i = 1 for spinal, i = 2 for rectangular, and i = 3 for globular shape). L is the inter-distance parameter of two adjacent NMI. L is a crucial component in determining the crack propagation between the two NMI that depends on the density of NMI (ρ). Generally, an increase in the density of NMI (ρ) decreases inter-distance among NMI (L), increasing the probability of cracking initiation ($\wedge$) as a result of reducing fracture toughness (K_{IC}). Further, B is a material constant, and n is the strain-hardening exponent. Based on Eqn. (1), it was concluded that the spinal NMI has a much larger contribution to the hydrogen-induced reduction of K_{IC} because these NMI are larger and closer to each other than other types of inclusions. Thus, spinal NMI reduces fracture resistance by introducing more nuclei for fracture initiation [82].

The distribution of NMI in steel plates is another factor affecting the susceptibility of pipeline steels to HIC. Domizzi and al. [86] and Rahman and al. [82] reported that most NMI with larger size and higher volume fractions are located in the middle thickness of steel pipes. This inhomogeneous distribution of NMI in the pipe suggests that there is a heterogeneity of fracture toughness, so the middle thickness of the pipe has lower fracture toughness and consequently a higher probability of hydrogen cracking than the regions near the surface. This conclusion is corroborated by the observation that most HIC cracks are located at the middle thickness of steel pipes.

Hydrogen trapping at the inclusion-matrix interface is also influenced by the elastic properties of the NMI and steel matrix. Peng and al. [20] and Qin and al. [85] proposed an elastic-energy-based model obtained from statistical information of NMI and the relation between hydrogen concentration at the inclusion-matrix interface and shear modulus. They concluded that an increase in shear elastic modulus of the matrix promotes hydrogen trapping, reducing the matrix ductility and concentrating elastic stresses around NMI. In such conditions, the HIC cracks initiate around NMI and easily propagate in the steel matrix [20, 85].

The crystallographic coherency of the inclusion-matrix interface is another factor that has been taken into consideration. In this regard, the lattice parameter of corresponding planes in NMI ($a_{inclusion}$) and matrix (a_{matrix}) determine the value of the elastic strain (f), as defined by Eqn. (2) [85].

$$f = \frac{a_{inclusion} - a_{matrix}}{a_{matrix}} \quad (2)$$

when NMI and steel matrix have the same crystallographic structure, crystallographic orientation, and lattice parameter, i.e., a fully coherent inclusion-matrix interface, the elastic strain at the interface has its lowest value [20, 84]. In general, the growth of NMI leads to loss of coherency, so the distribution of dissolved hydrogen atoms around the NMI change. When the length of NMI (L) is larger than the critical length (L_c), the hydrogen trapping and crack formation at interfaces depend on the density of misfit dislocations, and when an increase of misfit dislocation density reduces the number of dislocation loops around NMI, the process of plastic deformation is facilitated. Furthermore, when L is less than the L_c, the coherency is kept at the interface, and the coherency strain facilitates hydrogen trapping and, thus, enhances HIC [20, 85].

Chemical elements such as manganese, phosphorus, sulfur, nickel, chromium, niobium, vanadium, titanium, copper, calcium, and alloy carbide precipitations have an important role in determining hydrogen diffusion and NMI morphology. The susceptibility to HIC reduces with decreasing the content of manganese to less than 2 Wt. % [21]. Above 2 Wt. % manganese, high segregation ratio of manganese to carbon promotes HIC through hydrogen enhanced decohesion effect (HEDE), and hydrogen-enhanced- localized plasticity (HELP) [21]. Contents of phosphorus higher than 0.008 Wt. % reduce carbon activity in the presence of manganese, which enables higher contents of phosphorus migration to grain boundaries and thereby increases susceptibility to hydrogen cracking [21]. Additionally, low sulfur content enhances the ratio of longitudinal cracks in pipeline steels, promoting HIC [21]. Nickel reduces the hydrogen diffusion coefficient in the microstructure of pipeline steels [87, 88]. Additions of chromium of 0.3 Wt. % delay the eutectoid transformation of austenite and induce microstructural changes in the ferrite-pearlite and ferrite-bainite content, which indicates that by controlling the chromium content, the phase transformation temperature can be controlled to enhance HIC resistance. Additions of molybdenum of 0.4 Wt. % makes hydrogen absorption less likely, improving the HIC resistance of pipeline steels [21, 88]. Niobium and nanoscale particles of niobium carbide (NbC) and niobium nitride (NbN) disrupt dislocation interactions with hydrogen atoms and hinder crack propagation leading to the transition of intergranular fracture to microvoid coalescence, thus enhancing HIC resistance [89]. Nanoscale vanadium precipitations reduce hydrogen diffusion into the NMI and delay hydrogen cracking [90]. The effect of titanium addition on HIC resistance depends on the size of titanium carbide (TiC) and titanium nitride (TiN) particles. Titanium carbide and titanium nitride Ti (C, N) particles less than 0.1 μm diameter enhance HIC resistance [87, 88]. Contents above 0.2 Wt. % of copper improves the resistance of pipeline steels to HIC in the environment with a pH value greater than 4.0. This is because a stable copper-containing oxide film can be formed on the surface of the pipeline, reducing the permeation rate of hydrogen. Further, nanoscale copper-rich precipitates prevent redistribution of hydrogen atoms and improve resistance to HIC. Copper also affects the shape of ferrite, increasing copper content from 1 to 2 Wt. % modifies polygonal ferrite to acicular ferrite that has good HIC resistance; nonetheless, this may cause brittleness. Interaction between copper and cobalt can also decrease hydrogen uptake and thus reduce HIC susceptibility, while copper together with molybdenum has a detrimental effect on HIC resistance [21,23, 91]. The addition of calcium controls the shape of sulfide inclusions such as MnS and consequently improves HIC resistance. The calcium treatment maintaining the ratio of calcium to sulfur above 1.5 is suggested for pipeline steels with sulfur contents higher than 0.001 Wt.% [21].

Environment

Environmental factors such as pH and H_2S pressure critically affect hydrogen intake in pipeline steel. The decrease of pH and increase of pH_2S increase the generation of hydrogen atoms by anodic reaction of iron (Eqn. (3)) and the cathodic reaction of the hydrogen ion Eqn. (4)) [92].

$$Fe \rightarrow Fe^{2+} + 2e \quad (3)$$

$$2H^{+} + 2e \rightarrow 2H \text{ (Atomic hydrogen)} \rightarrow H_2 \quad (4)$$

where hydrogen ions can be generated by dissociation reactions; (Eqn. (5)):

$$H_2S \rightarrow H^+ + HS^- \quad (5)$$

The diffusion of hydrogen atoms into the interstitial lattice sites and inclusion-matrix interface increases hydrogen pressure decreasing the strength of interatomic bonds (cohesive strength) along the grain boundaries and promoting HIC by a mechanism known as the hydrogen-enhanced decohesion (HEDE) [93]. Fig. 6 depicts a schematic illustration of HEDE. To fully understand this result, Eqn. (6) shows that the pH and pH_2S are the main environmental parameters at ambient temperature affecting hydrogen flux (J_{Perm}) and HIC resistance [94]. Generally, the increase of p_{H2S} and the decrease of pH increase hydrogen permission flux and hydrogen gas pressure into the crack cavity, resulting in the growth of HIC crack and then the decrease of HIC resistance.

$$J_{perm} = K(d)\left(p_{H_2S}\right)^{0.25} 10^{-0.17pH} \quad (6)$$

where the value of K(d) is determined from experimental data of Kittel and al. [95] and depends on corrosion layer thickness (d).

Residual stress

Steel manufacturing processes such as machining, joining, and rolling have considerable influence on residual stress and strain distribution in steel plates used to manufacture seam pipes for hydrocarbon transport. Indeed, heterogeneous residual stress fields and plastic strains caused by inhomogeneous plastic deformation affect hydrogen permeation and HIC fracture susceptibility as proposed by Kharin and Toribio [96]. Jack and al. [97] showed that a high level of residual stress, consequently high dislocations density, and the high-volume fraction of high angle grain boundaries led to the hydrogen-induced fracture in X65 pipeline steel. Therefore, a precise temperature schedule during TMCP and selection of the proper welding procedure effectively reduces residual stress in pipeline steels [97]. The welding joints of pipeline steels also produce residual stress in the weld metal and the heat-affected zone where hydrogen accumulation and then hydrogen cracking occur. Javadi and al. [98] proposed that hydrogen concentration decreased as the distance from the weld metal increased.

PREDICTION OF HIC GROWTH RATES

Phenomenological methods

Phenomenological methods have been applied to predict the HIC growth rate in order to develop the FFS assessment criteria for in-service pipelines and to mitigate hydrogen-induced fracture risk [29]. According to the hydrogen pressure mechanism (HPT), the concentration of the atomic hydrogen within trapping sites, such as grain boundaries and internal voids, leads to increased pressure at the cavity, which eventually causes the formation of an embedded crack and thereby initiating hydrogen-induced cracking [99]. Another suggested mechanism of hydrogen damage is the hydrogen-enhanced decohesion model (HEDE), which assumes that HIC is caused by the diffusion of atomic hydrogen into the interstitial sites, decreasing the strength of interatomic bonds (cohesive strength) along the grain boundaries and resulting in hydrogen cracking, as schematically shown in Fig. 6 [100, 101].

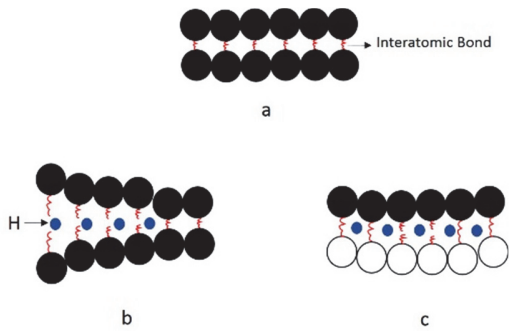

Figure 6: Schematic of hydrogen-enhanced decohesion (HEDE). a) atomic lattice b) absorbed hydrogen c) hydrogen at particle-matrix interfaces.

Hydrogen-enhanced localized plasticity (HELP) establishes that HIC is caused by hydrogen adsorption into a preexisting crack cavity leading to adsorption-induced dislocation emission (AIDE), as schematically shown in Fig. 7. The accumulation of hydrogen atoms in the crack cavity reduces the plastic zone size around the crack tip, which results in high local triaxial stresses that induce microvoid coalescence and further crack growth [102].

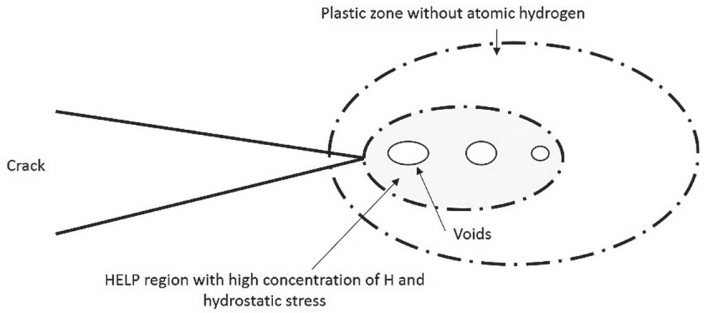

Figure 7: Effect of hydrogen adsorption on the area of the plastic zone as hydrogen-enhanced localized plasticity (HELP) mechanism.

HEDE and HELP mechanisms are primarily related to the final fracture mode, whereas HPT is related to the initiation and stable growth of HIC. Robertson and al. [103] proposed that the transition from HELP to HEDE mechanism occurs in areas with a high concentration of hydrogen.

In general, the phenomenological models attempt to correlate HIC growth rate with critical strain energy release rate, yield stress, hydrogen-induced fracture toughness, and hydrogen diffusion within the crack opening. The yield stress (σ_y) and plastic strain (ε_P) and plain strain fracture toughness (K_{IH}) of steels exposed to the atomic hydrogen depend on hydrogen concentration (C) while Young's module (E) is little affected, and these effects have to be introduced in the models. Generally, the yield stress and fracture toughness of steels exposed to hydrogen charging environments decreases with the increase of hydrogen concentrations into hydrogen trap sites.

Huang and al. [104] and Sofronis and al. [105] proposed a phenomenological model based on the HEDE mechanism in which the critical energy release rate ($\overline{G}_c$) is a function of hydrogen concentration, as represented by Eqn. (7) and Eqn. (8). A high $\overline{G}_c$ value may suppress crack initiation under elastic deformation and promote ductile fracture.

$$\overline{G}_c = G_c(C) \tag{7}$$

$$G_c(C) = \begin{cases} [(\zeta-1)\dfrac{C}{C_0}]\, G_c & G_c(C) > \zeta G_c \\ \zeta G_c & G_c(C) \le \zeta G_c \end{cases} \tag{8}$$

where C is the total hydrogen concentration, C_0 is the initial hydrogen concentration, G_c (C) represents the embrittlement function. ζ and ξ are parameters that control the initial and the maximum reduction of the critical energy release rate, with ξGc denoting a lower bound value. The values of ζ and ξ are 0.9-0.8 and 0.5, respectively [104, 105].

Furthermore, the crack driving force function ($\overline{H}$) is presented by Eqn. (9) [104, 105]:

$$\overline{H} = \frac{\psi^{e^+}}{\overline{G}_c / LA} \tag{9}$$

where $\overline{G}_c$ is critical energy release rate, L is a length scale parameter controlling the smoothness of the crack topology, and A and ψ^{e^+} represent plastic adjustment function and density of stored elastic energy, respectively, as defined by Eqn. (10) and Eqn. (11) [104, 105]:

$$A = exp\left(\frac{a\,\bar{\varepsilon}_p}{\varepsilon_f}\right) \tag{10}$$

$$\psi^{e^+} = K\left\langle tr(\varepsilon)\right\rangle_+^2 + 2\mu\,(\varepsilon^e_{dev} : \varepsilon^e_{dev}) \tag{11}$$

In the above equations, the coefficient α is a material parameter, $\bar{\varepsilon}_P$ is the equivalent plastic strain, and ε_f is a critical failure strain. The bracket $\langle X\rangle_+$ is viewed as a function of $(X \pm |X|) / 2$, K denotes the bulk modulus, and μ is the shear modulus. Also, tr (ε) expresses the trace of the strain tensor, and ε^e_{dev} is the elastic part of the deviatoric strain tensor expressed as $\varepsilon^e_{dev} = \varepsilon^e - tr(\varepsilon)\, I/3$ with ε^e and I signifying the elastic strain and second-order identity tensor, respectively [104, 105]. The above phenomenological model incorporated plastic contribution into the crack driving force function, assuming a higher critical energy release rate and consequently lower crack driving force for ductile fracture [104, 105]. This model can predict crack initiation and propagation and brittle-ductile transition in the fracture of pipeline steels.
Sofronis and al. [105] and Liang and al. [106] suggested a HELP model that describes the hydrogen effect on the local yield stress (σy) as presented by Eqn. (12):

$$\sigma_y = \sigma_0^H \left(1 + \frac{\varepsilon_P}{\varepsilon_0}\right)^{\frac{1}{n}} \tag{12}$$

where σ_0^H is the initial yield stress in the presence of hydrogen, ε_P is the plastic strain in uniaxial tension, ε_0 is the initial yield strain in the absence of hydrogen and n is the hardening exponent that is assumed unaffected by hydrogen.
Gerberich and al. [107, 108] proposed a model that calculates HIC crack growth in correlation with plane strain fracture toughness (K_{IH}) and grain size (d) in the form of the differential equations:

$$\frac{da}{dt} = \frac{2(1+\vartheta)\, C_0 D_{eff} \bar{V}_H\, K_{IH}}{3\, d^{1.5} R\, T\, (C_{Crit} - C_0)} \tag{13}$$

The correlation of stable hydrogen crack growth with yield stress (σ_y) and grain size (d) is:

$$\frac{da}{dt} = \frac{9\, C_0 D_{eff} \bar{V}_H\, \sigma_y}{2\, d\, R\, T (C_{Crit} - C_0)} \tag{14}$$

The unstable hydrogen cracks growth in correlation with plane strain fracture toughness (K_{IH}) and grain size (d) is given by:

$$\frac{da}{dt} = \frac{9 C_0\, D_{eff} \bar{V}_H\, K_{IH}^2}{2E d^2 R\, T (C_{Crit} - C_0)} \tag{15}$$

where C_0 is the initial hydrogen concentration, C_{Crit} is the critical hydrogen concentration, D_{eff} is the diffusivity of hydrogen in steel, $\bar{V}_H$ is hydrogen partial molar volume in steel, E is Young's module, ϑ is Poisson's ratio, and R and T are the universal gas constant, ambient temperature, respectively.
These authors [107, 108] proposed a formula (Eqn. 16)) to calculate the time required to crack initiation in correlation with yield stress and stress concentration factor (K):

$$t_1 = \frac{C_1}{K} \times \rho^{0.5} \times \left[C_2 \left(1 - \frac{K}{2(\sigma_y \times E)^{0.5}} \right)^2 - 1 \right]^{\frac{5}{4}} \tag{16}$$

where C_1 is the diffusivity constant, C_2 is a constant determined by the correlation between fracture stress and hydrogen embrittlement and ρ is Notch root radius.

A phenomenological model proposed by Gonzalez and al. [17] assumed that the HIC crack growth results from the accumulation of internal hydrogen pressure in a preexisting cavity that increases the stress intensity factor, and when it surpasses the plane strain fracture toughness of steel with dissolved hydrogen in the fracture plane, the crack propagates. They proposed a model that predicts HIC crack growth rate based on the fracture mechanics criterion that establishes that the crack will start to grow when the plane strain fracture toughness in the cracking plane (K_{IH}) reaches its critical value, Eqn. 17.

$$K_{IH} = 2p_{H2}\sqrt{\frac{a}{\pi}} \tag{17}$$

where p_{H2} is atomic hydrogen pressure and a is the crack length. Solving Eqn. 18 for the crack length and obtaining the total differential equation, Gonzalez and al. [17] reached the following equation for the HIC crack growth rate:

$$\frac{da}{dt} = \left[\frac{3\,\alpha\,R\,T\,E'\,D_H\bar{V}_H\Delta C_H}{4\,K^2_{IH}\,B}\right]a \tag{18}$$

where ΔC_H is the hydrogen concentration gradient, D_{eff} is the diffusivity of hydrogen in steel, and B is the wall thickness, and R, T, and $\bar{V}_H$ are the universal gas constant, ambient temperature, and hydrogen partial molar volume in steel, respectively. Also, the constant α is 11.5 for P= 17500 atm and $E' = \frac{E}{1-\nu^2}$.

The HIC crack length after exposure time (t) to the hydrogen charging environment is defined by Eqn. (19).

$$a = a_0\, e^{Ht} \tag{19}$$

where a_0 is the initial crack length at time t = 0 and H is:

$$H = \left[\frac{3\,\alpha\,R\,T\,E'\,D_H\Delta C_H}{4\,K^2_{IH}\,B}\right] \tag{20}$$

According to this model, the HIC crack growth rate will be faster as K_{IH} decreases, while a high value of D_H and ΔC_H will increase the crack growth rate, which is logical since these two parameters indicate the input flux of hydrogen, so the higher input, the higher HIC rate.

Further, Gonzalez and al. [17] investigated the mechanism and kinetics of HIC by cathodic charging experiments, finding that HIC cracks mainly initiate at the interface of elongated MNS and steel matrix, and they propagate in a path parallel to the rolling direction along with the interfaces of pearlite and ferrite bands. They also showed that the shape of HIC cracks is conditioned by the spatial distribution of HIC nuclei, namely non-metallic inclusions, and it is less affected by microstructural anisotropy. However, after some time, the individual cracks begin to interconnect to form large cracked areas with a drastic decrease in the HIC growth rate. According to their findings, Gonzalez and al. [17] demonstrated that HIC occurs in two stages; nucleation and growth of individual cracks, where the maximum HIC growth rate is observed, and the second is the interconnection of individual cracks where the kinetics is slowed down to almost zero. However, the phenomenological model presented by Gonzalez and al. [17] did not consider the interconnection stage; nonetheless, it showed a good correlation with the observed experimental HIC growth rates of individual cracks. Fig. 8 shows the comparison of experimental results and the tendency of HIC kinetics predicted with Gonzalez's model [17], good agreement between experimental and predicted results [109].

Diniz and al. [110] suggested a phenomenological model considering the hydrogen transport through interstitial diffusion, as shown in Eqn. (21).

$$\frac{dc_t}{dt}=\frac{C_h-C_t}{\tau_D}+\frac{C_{b-C_t}}{\lambda_D}\frac{da}{dt} \tag{21}$$

where λ_D denotes the length of the diffusion zone, a represents the crack length, and τ_D is diffusion time. C_t represents hydrogen concentration at the crack tip, and C_h indicates the hydrogen concentration for the stationary crack when $t>>\tau_D$, and C_b is the hydrogen concentration for fast crack propagation [110].

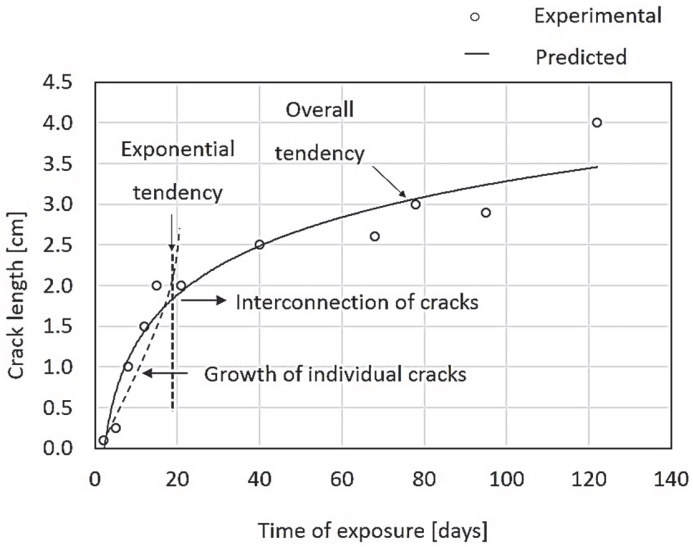

Figure 8: Comparison of experimental and predicted results of HIC growth of an API 5L X52 steel plate by cathodic charging and a synthetic sour medium.

Hydrogen transport through the hydrogen trapping mechanism was modeled by MC-Nabb and Foster [111] and is represented by Eqn. (22).

$$\frac{\partial\theta_T}{\partial t}=KC_L\left(1-\theta_T\right)-\rho\theta_T \tag{22}$$

where C_L is hydrogen concentration in normal interstitial lattice sites, θ_T denotes the coverage of trapping sites, K represents the hydrogen capture rate, and ρ is the hydrogen release rate.

It should be noted that the above model describes the threshold hydrogen concentrations at the crack tip.

Balueva [112] proposed a phenomenological model based on determining the time to grow delamination (t) under hydrogen pressure, given by Eqn. 23:

$$t=2\alpha\left(a-\frac{1}{2}\frac{\beta a}{a^2+\beta}-\frac{1}{2}\sqrt{\beta}\arctan\left(\frac{a}{\sqrt{\beta}}\right)\right) \tag{23}$$

where α and β are defined as:

$$\alpha=\frac{\pi G_C}{6RTC_0D_{eff}} \tag{24}$$

$$\beta=8B_2\sqrt{2G_CD_0} \tag{25}$$

G_c is the critical energy release rate specified as:

$$G_C = \frac{p_{H2}^2 a^4}{128 D_0} \tag{26}$$

where P_{H2} is atomic hydrogen pressure, a is delamination radius and D_0 is flexural rigidity defined by Eqn. 27:

$$D_0 = \frac{Eh^3}{\left(\left[12\left(1-\upsilon^2\right)\right]\right)} \tag{27}$$

where h is a thin layer of thickness, E is Young's modulus, and υ is the Poisson ratio.
Delamination radius (a) under hydrogen pressure overtime is defined by Eqn. 28:

$$a(t) = \frac{1}{2\alpha} t + \frac{1}{4}\pi\sqrt{\beta} \tag{28}$$

Empirical models

Traidia and al. [94, 113] presented an empirical model considering the effect of temperature on HIC growth rate. They found a decrease in temperature at range 0-100 °C for an aggressive environment (pH = 3 and pH_2S = 1000 mbar) decreased the mechanical properties of steels, especially the fracture toughness and increased hydrogen pressure in the crack cavity. The combination of these two factors causes HIC to develop mainly at low temperatures; however, hydrogen cracking is not observed at a temperature higher than 65 °C [113].
According to these authors [94, 113], the hydrogen cracks growth rate is related to fracture toughness (K_{IH}) and p_{H2}, given by the differential equations:

$$\frac{da}{dt} = \frac{2a}{p_{H2}} \frac{dp_{H2}}{dt} + \frac{\pi E}{4\left(1-\vartheta^2\right)p_{H2}^2} \frac{dK_{IH}}{dC_{ct}} \frac{dC_{ct}}{dt} \tag{29}$$

where C_{ct} is the hydrogen concentration at the crack tip, while p_{H2} is defined as:

$$p_{H2} = \frac{n_{H2} RT}{V - n_{H2} RTB} \tag{30}$$

where n_{H2} is the total number of hydrogen moles, V is the crack volume determined by integration of the crack opening, T is temperature, and B is given by Eqn. 31:

$$B = \frac{z_1}{T} + z_2 \tag{31}$$

where Z_1 is the first compressibility constant (1.54×10^{-6} K Pa^{-1}), and Z_2 is the second compressibility constant (4.69×10^{-8} K Pa^{-1}), p_{H2} is a function of t, and p_{H2} is a function of K_{IH} as follows:

$$P(t) = \frac{C_{cs}(t)^2}{\gamma(P,T)\, S(T)^2} \tag{32}$$

$$p_{H2}^{Crit} = \frac{\pi K_{IH}}{2\sqrt{\pi a}} \tag{33}$$

The hydrogen concentration at the crack surface (Ccs) is defined by Eqn. 34:

$$C_{CS}=S(T)\exp\left(\frac{\sigma_h \bar{V}_H}{RT}\right)\sqrt{p_{H2}\,(\gamma(P,T))} \tag{34}$$

where hydrogen solubility (S) and fugacity factor of gaseous hydrogen (γ (P, T)) are represented by the below equations:

$$S(T)= S_0 \exp\left(\frac{-\Delta H_S}{RT}\right) \tag{35}$$

$$\gamma(P,T)=\exp\left[\left(\frac{Z_1}{T}+ Z_2\right) p_{H2}\right] \tag{36}$$

Where S_0 is the hydrogen solubility pre-exponential factor (0.82 mol/($m^3Pa^{-1/2}$)[12]), and ΔH_S is the enthalpy of solution (28.6 kJ mol^{-1}).
In more recent work, Gonzalez and Rivas and al. [114] developed an empirical HIC growth rate model based on the best-fit curve of experimental data, which is presented in Eqn. (37).

$$A=A(i)^* e^{-e^{\frac{t-\mu_i}{\sigma(i)}}} \tag{37}$$

where t is the cathodic charging time and also $A(i)^*$, σ_i and μ_i, which are a function of the applied current density (i)are defined by the below equations:

$$A(i)^* = A_{max} - \beta i^2 \tag{38}$$

$$\sigma_i = \alpha e^{-\gamma i^2} \tag{39}$$

$$\mu_i = \delta e^{-\eta i^2} \tag{40}$$

Parameters α, β, γ, δ and η are material constants that have to be found experimentally for every specific steel since these are parameters dependent on the microstructure, volume and shape of non-metallic inclusions, strength and chemical composition of the steel [114].
Fig. 9 shows a comparison of experimental and simulated results of HIC growth of an API 5L X60 steel plate, reported by Traidia and al. [94]. They compared the numerical predictions of HIC kinetics in two different K_{IH} with the experimental data achieved by Brouwer and al. [115] and found a good agreement on both the HIC initiation and growth of simulated and experimental results, see Fig. 9.

Further considerations to establish HIC models

The ample evidence available nowadays makes it possible to use the multi-physics models to predict hydrogen cracking behavior in pipeline steels. This evidence indicates that the hoop stress induced by the internal pressure, crystallographic texture, and the tensile mechanical properties, along with the geometry and location of the HIC cracks and the pipe thickness, have a little effect on the kinetics of hydrogen cracking in pipeline steels. However, hydrogen permeation rate, the nature and spatial distribution of non-metallic inclusions, in-plane fracture toughness, and the individual crack interconnection events are among the main parameters to establish a comprehensive HIC kinetics model.
At the service temperatures of most hydrocarbon pipelines, pH and pH_2S are the two main operational parameters that control the HIC kinetics since they directly affect the hydrogen permeation rates. Indeed, the experimental evidence shows that lower pH and higher pH_2S decrease the incubation period. The incubation period is the time needed to reach the critical pressure for the HIC cracks growth [27, 116]. However, the few available experimental data and in-field evidence indicate that incubation times are a few hours or even less than an hour. Therefore, attention has to be placed on the active propagation of already formed HIC cracks.

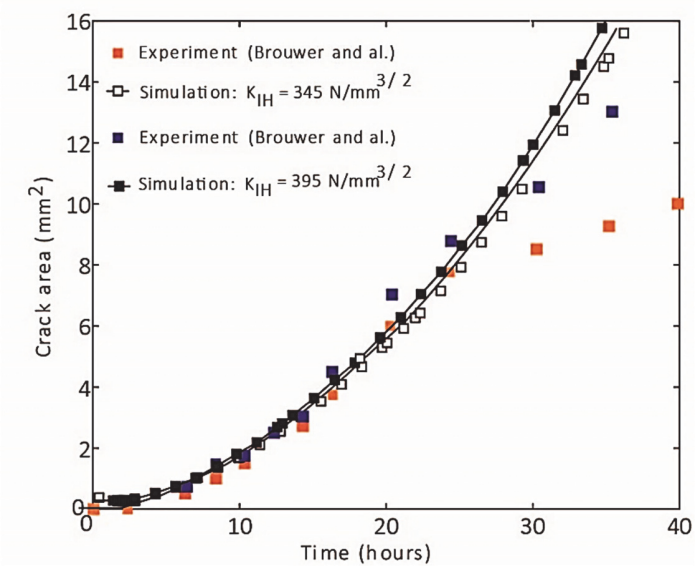

Figure 9: Comparison of experimental and simulated results of HIC growth of an API 5L X60 steel plate.

The nature and distribution of NMI control the kinetics of HIC cracks of steel pipe by determining the number and separation of initial HIC cracks. As observed in this paper, larger inclusions with spinal morphologies that are commonly observed in the middle thickness of steel pipes contribute to low fracture toughness and more numerous initial cracks, which lead to higher kinetics of HIC. So, in modeling the kinetic of HIC, the role of NMI with respect to spatial distribution and nature should be considered to establish a reliable model.

Another important consideration is the interconnection of HIC cracks which is an inevitable condition after the individual cracks have reached the necessary sizes to interconnect to each other. The experimental observations performed by Gonzalez and al. [17] indicate that the more initial HIC cracks, the shorter time to begin the interconnection stage, which is only a few days in some cases. Furthermore, the model has to incorporate the new HIC cracks that continue to appear after several weeks or even months of exposure to hydrogen charging environment, a phenomenon that has been little investigated, i.e., the delayed nucleation of HIC cracks.

SUMMARY AND CONCLUSIONS

Heat treatments, microstructures, especially nature and spatial distribution of non-metallic inclusions, hydrogen permeation rate, and the mechanical and fracture mechanics properties are the key factors affecting the kinetics of HIC.

Thermomechanical controlled processing (TMCP) is the main processing route for manufacturing the HSLA steel pipes with good mechanical properties and high HIC resistance. In this regard, controlling various temperature parameters during TMCP, such as preheating temperature, Tnr, FCT, and FRT, leads to microstructural refinement and consequently improves HIC resistance.

Regarding microstructure, pearlitic and martensitic microstructures are susceptible to HIC cracking; however, granular bainite and tempered martensite positively influence the HIC resistance. Another important microstructural factor is also the nature and spatial distribution of non-metallic inclusions. Larger inclusions with spinal and rectangular morphologies are the main nuclei for HIC, and additionally, contribute to the degradation of fracture toughness and increasing kinetic of HIC. Furthermore, the growth of non-metallic inclusions increases the density of misfit dislocations, which plays the main role in hydrogen trapping rate and facilitates plastic deformation and, thus, HIC growth at the inclusion-matrix interface. Further, as another microstructural factor, alloying elements such as manganese (less than 2 Wt. %), chromium (Less than 0.3 Wt. %), molybdenum (Less than 0.4 Wt. %), phosphorus (Less than 0.008 Wt. %), copper (above 0.2 Wt.%), and calcium, as well as carbide precipitations enriched with niobium, vanadium, and titanium enhance HIC resistance in pipeline steels.

The pH and pH_2S are the environmental factors affecting the hydrogen permission rate. Generally, the decrease of pH and increase of pH_2S increase hydrogen permission rate through the generation of hydrogen atoms by anodic reaction of iron and the cathodic reaction of the hydrogen ion. The diffusion of hydrogen atoms into the hydrogen trap sites, especially the

inclusion-matrix interface, increases hydrogen pressure and, thus, HIC initiation and growth. Moreover, heterogeneous residual stress fields generated by an inappropriate manufacturing process are known as a parameter increasing hydrogen permeation rate and HIC fracture susceptibility.
The yield stress (σ_y) and fracture toughness (K_{IH}) of steels exposed to the atomic hydrogen depends on hydrogen concentration stored into hydrogen trap sites; the increase of hydrogen concentration, the decrease of yield stress and fracture toughness, and thus, the HIC crack growth rate will be faster.

ACKNOWLEDGMENT

The authors E. Entesari, J.L. Gonzalez and D. Rivas are grateful to Instituto Politécnico Nacional (IPN) and CONACYT for their financial support.

REFERENCES

[1] Scherf, S., Harksen, S., Hojda, R., Strötgen, D. (2018).Weldability of High Toughness X100 Seamless Pipes With a New Low Carbon Alloying Concept for Arctic Offshore Structural Applications. The 28th International Ocean and Polar Engineering Conference, OnePetro.
[2] Carrasco, J.P., Diniz, D.D.S., Barbosa, J.M.A., Silva, A.A., dos Santos, M.A. (2019). Numerical simulation of the hydrogen trapping effect on crack propagation in API 5CT P110 steel under cathodic overprotection, Int. J. Hydrogen Energy, 44(5), pp. 3230-3239.
[3] Da Trindade Filho, V.B., SILVA, J.M.S.E., Linne, C., BOAS, A.C.C.V. (2020). High strength micro alloyed steel seamless pipe for sour service and high toughness applications.
[4] Morales, E. V., Bott, I.S., Silva, R.A., Morales, A.M., de Souza, L.F.G. (2016). Characterization of carbon-rich phases in a complex microstructure of a commercial X80 pipeline steel, J. Mater. Eng. Perform., 25(7), pp. 2736–2745.
[5] Stalheim, D.G., Muralidharan, G. (2006).The role of continuous cooling transformation diagrams in material design for high strength oil and gas transmission pipeline steels. International Pipeline Conference, 42630, pp. 231–238.
[6] Javaheri, V., Pohjonen, A., Asperheim, J.I., Ivanov, D., Porter, D. (2019). Physically based modeling, characterization and design of an induction hardening process for a new slurry pipeline steel, Mater. Des., 182, pp. 108047.
[7] Alaneme, K.K., Olanrewaju, S.O., Bodunrin, M.O. (2011). Development and Performance Evaluation of a Salt Bath Furnace., Int. J. Mech. Mater. Eng., 6(1), pp. 67-74.
[8] Shikanai, N., Mitao, S., Endo, S. (2008). Recent development in microstructural control technologies through the thermo-mechanical control process (TMCP) with JFE steel's high-performance plates, JFE Tech. Rep., 11(6), pp. 1-6.
[9] Zhao, M.-C., Yang, K., Shan, Y. (2002). The effects of thermo-mechanical control process on microstructures and mechanical properties of a commercial pipeline steel, Mater. Sci. Eng. A, 335(1–2), pp. 14-20.
[10] Jiang, M., Chen, L.-N., He, J., Chen, G.-Y., Li, C.-H., Lu, X.-G. (2014). Effect of controlled rolling/controlled cooling parameters on microstructure and mechanical properties of the novel pipeline steel, Adv. Manuf., 2(3), pp. 265-274.
[11] Zikeev, V.N., Chevskaya, O.N., Mishet'yan, A.R., Filippov, V.G., Korostelev, A.B. (2021). Effect of High Strength Structural Steel Structural State on Fracture Resistance, Metallurgist, 65(3), pp. 375-388.
[12] Koo, J.Y., Luton, M.J., Bangaru, N. V., Petkovic, R.A., Fairchild, D.P., Petersen, C.W., Asahi, H., Hara, T., Terada, Y., Sugiyama, M. (2003).Metallurgical design of ultra-high strength steels for gas pipelines. The Thirteenth International Offshore and Polar Engineering Conference, OnePetro.
[13] Askari, M., Aliofkhazraei, M., Afroukhteh, S. (2019). A comprehensive review on internal corrosion and cracking of oil and gas pipelines, J. Nat. Gas Sci. Eng., 71, pp. 102971.
[14] NACE International the Corrosion Society. (2016). Nace standard TM0284: standard test method evaluation of pipeline and pressure vessel steels for resistance to Hydrogen-Induced Cracking.
[15] NACE International the Corrosion Society. (2005). ANSI/NACE TM0177: Laboratory Testing of Metals for Resistance to Sulfide Stress Cracking and Stress Corrosion Cracking in H_2S Environments.
[16] NACE International the Corrosion Society. (2003). NACE standard TM0103: Laboratory Test Procedures for Evaluation of SOHIC Resistance of Plate Steels Used in Wet H_2S Service.
[17] Gonzalez, J.L., Ramirez, R., Hallen, J.M., Guzman, R.A. (1997). Hydrogen-induced crack growth rate in steel plates exposed to sour environments, Corrosion, 53(12).

[18] Arafin, M.A., Szpunar, J.A. (2011). Effect of bainitic microstructure on the susceptibility of pipeline steels to hydrogen induced cracking, Mater. Sci. Eng. A, 528(15), pp. 4927-4940.
[19] Moon, J., Choi, J., Han, S.-K., Huh, S., Kim, S.-J., Lee, C.-H., Lee, T.-H. (2016). Influence of precipitation behavior on mechanical properties and hydrogen induced cracking during tempering of hot-rolled API steel for tubing, Mater. Sci. Eng. A, 652, pp. 120-126.
[20] Peng, Z., Liu, J., Huang, F., Hu, Q., Cao, C., Hou, S. (2020). Comparative study of non-metallic inclusions on the critical size for HIC initiation and its influence on hydrogen trapping, Int. J. Hydrogen Energy, 45(22), DOI: 10.1016/j.ijhydene.2020.02.131.
[21] Ghosh, G., Rostron, P., Garg, R., Panday, A. (2018). Hydrogen induced cracking of pipeline and pressure vessel steels: A review, Eng. Fract. Mech., 199, pp. 609–618.
[22] Hsu, Y.-T., Jiang, H.-Y., Yen, H.-W., Lin, H.-C., Hong, S. (2020). Hydrogen-induced embrittlement of nickel-chromium-molybdenum containing HSLA steels, J. Chinese Inst. Eng., 43(1), pp. 58-66.
[23] Shi, X., Yan, W., Wang, W., Shan, Y., Yang, K. (2016). Novel Cu-bearing high-strength pipeline steels with excellent resistance to hydrogen-induced cracking, Mater. Des., 92, pp. 300-305.
[24] Lin, L., Li, B., Zhu, G., Kang, Y., Liu, R. (2018). Effect of niobium precipitation behavior on microstructure and hydrogen induced cracking of press hardening steel 22MnB5, Mater. Sci. Eng. A, 721, pp. 38-46.
[25] González-Velázquez, J.L., Entezari, E., Szpunar, J.A. (2022). On the Assessment of non-metallic inclusions by part 13 of API 579-1/ASME FFS-1 2016., Frat. e Integrita Strutt., (59).
[26] Turk, A., San Martín, D., Rivera-Díaz-del-Castillo, P.E.J., Galindo-Nava, E.I. (2018). Correlation between vanadium carbide size and hydrogen trapping in ferritic steel, Scr. Mater., 152, pp. 112-116.
[27] Mohtadi-Bonab, M.A., Eskandari, M. (2017). A focus on different factors affecting hydrogen induced cracking in oil and natural gas pipeline steel, Eng. Fail. Anal., 79, DOI: 10.1016/j.engfailanal.2017.05.022.
[28] Li, X., Xie, F., Wang, D., Xu, C., Wu, M., Sun, D., Qi, J. (2018). Effect of residual and external stress on corrosion behaviour of X80 pipeline steel in sulphate-reducing bacteria environment, Eng. Fail. Anal., 91, pp. 275-90.
[29] Traidia, A., Chatzidouros, E., Jouiad, M. (2018). Review of hydrogen-assisted cracking models for application to service lifetime prediction and challenges in the oil and gas industry, Corros. Rev., 36(4), pp. 323-47.
[30] Boellinghaus, T., Hoffmeister, H. (2000). Numerical model for hydrogen-assisted cracking, Corrosion, 56(06),.
[31] HKDH Bhadeshia. HKDH Bhadeshia.(n.d.). Materials Algorithms Project. Available at: https://www.phase-trans.msm.cam.ac.uk/map/steel/programs/mucg83.html.
[32] Sente Software Ltd. Sente Software Ltd.(n.d.). JMatPro®. Available at: http://www.jmatpro.com.
[33] software Development Kits. software Development Kits. (n.d.). Thermo-Calc Software AB. Available at: http://www.thermocalc.com/ Products- services/software-development-kits.
[34] Yamashita, T., Okuda, K., Obara, T. (1999). Application of thermo-calc to the developments of high-performance steels, J. Phase Equilibria, 20(3), pp. 231-237.
[35] Lin, L.I., Yanlin, H.E., De Cooman, B.C., Wollants, P., Huang, S.G., Vleugels, J. (2006). Computer-aided designing and manufacturing of advanced steels, Rare Met., 25(5), pp. 407-411.
[36] Chen, Y., Zhou, X., Huang, J. (2019). Chemical Component Optimization Based on Thermodynamic Calculation of Fe-1.93 Mn-0.07 Ni-1.96 Cr-0.35 Mo Ultra-High Strength Steel, Materials (Basel)., 12(1), pp. 65.
[37] Vervynckt, S. (2010). Control of the Non-Recrystallization Temperature in High Strength Low Alloy (HSLA) Steels.
[38] Liessem, A., Knauf, G., Zimmermann, S. (2007).Strain based design-what the contribution of a pipe manufacturer can be. The Seventeenth International Offshore and Polar Engineering Conference, OnePetro.
[39] Rosado, D.B., De Waele, W., Vanderschueren, D., Hertelé, S. (2013). Latest developments in mechanical properties and metallurgical features of high strength line pipe steels, Int. J. Sustain. Mech. Eng. Des., 4(1).
[40] Liu, C., Bhole, S.D. (2013). Challenges and developments in pipeline weldability and mechanical properties, Sci. Technol. Weld. Join., 18(2), pp. 169-181.
[41] Yoo, J.-Y., Ahn, S.-S., Seo, D.-H., Song, W.-H., Kang, K.-B. (2011). New development of high grade X80 to X120 pipeline steels, Mater. Manuf. Process., 26(1), pp. 154-160.
[42] Yang, X.-L., Xu, Y.-B., Tan, X.-D., Wu, D. (2015). Relationships among crystallographic texture, fracture behavior and Charpy impact toughness in API X100 pipeline steel, Mater. Sci. Eng. A, 641, pp. 96-106.
[43] (N.d.). Substances and technologies, Knowledge source on materials engineering.
[44] Zhang, K., Zhu, M., Lan, B., Liu, P., Li, W., Rong, Y. (2019). The Mechanism of High-Strength Quenching-Partitioning-Tempering Martensitic Steel at Elevated Temperatures, Crystals, 9(2), pp. 94.
[45] Entezari, E., Mousalou, H., Yazdani, S., González-Velázquez, J.L., Szpunar, J.A. (2022). The Evaluation of Quenching Temperature Effect on Microstructural and Mechanical Properties of Advanced High Strength Low Carbon Steel After

Quenching Partitioning Treatment, Procedia Struct. Integr., 37, pp. 145-52.
[46] Zhao, J., Jiang, Z. (2018). Thermomechanical processing of advanced high strength steels, Prog. Mater. Sci., 94, pp. 174-242.
[47] Ohaeri, E., Omale, J., Tiamiyu, A., Rahman, K.M.M., Szpunar, J. (2018). Influence of thermomechanically controlled processing on microstructure and hydrogen induced cracking susceptibility of API 5L X70 pipeline steel, J. Mater. Eng. Perform., 27(9), pp. 4533-4547.
[48] Hwang, B., Kim, Y.M., Lee, S., Kim, N.J., Ahn, S.S. (2005). Correlation of microstructure and fracture properties of API X70 pipeline steels, Metall. Mater. Trans. A, 36(3), pp. 725-739.
[49] Min, Z. (2010). Microstructure and mechanical properties of X80 pipeline steels in different cooling schedules, Acta Metall. Sin. (English Lett., 23(3), pp. 171-175.
[50] Yu, Q.B. (2012).Effect of cooling rate on microstructures and mechanical properties of X80 pipeline steel. Advanced Materials Research, vol. 535, Trans Tech Publ, pp. 525–528.
[51] Zhao, J., Hu, W., Wang, X., Kang, J., Cao, Y., Yuan, G., Di, H., Misra, R.D.K. (2016). A Novel thermo-mechanical controlled processing for large-thickness microalloyed 560 MPa (X80) pipeline strip under ultra-fast cooling, Mater. Sci. Eng. A, 673, pp. 373-377.
[52] Lan, L., Chang, Z., Kong, X., Qiu, C., Zhao, D. (2017). Phase transformation, microstructure, and mechanical properties of X100 pipeline steels based on TMCP and HTP concepts, J. Mater. Sci., 52(3), pp. 1661-1678.
[53] Lee, D.H., Sohn, S.S., Song, H., Ro, Y., Lee, C.S., Lee, S., Hwang, B. (2018). Effects of start and finish cooling temperatures on the yield strength and uniform elongation of strain-based API X100 pipeline steels, Metall. Mater. Trans. A, 49(10), pp. 4536-4543.
[54] Nafisi, S., Arafin, M.A., Collins, L., Szpunar, J. (2012). Texture and mechanical properties of API X100 steel manufactured under various thermomechanical cycles, Mater. Sci. Eng. A, 531, pp. 2-11.
[55] Zhou, X., Zeng, C., Yang, H., Ma, L., Liu, Z., Wu, D., Wang, G. (2016). Effect of cooling process on microstructure and mechanical properties of X100 pipeline steel, Steel Res. Int., 87(10), pp. 1366-1375.
[56] Takeuchi, I., Makino, H., Okaguchi, S., Takahashi, N., Yamamoto, A. (2006).Crack arrestability of high-pressure gas pipelines by X100 or X120. 23rd World Gas Conference, Amsterdam, Citeseer, pp. 1-16.
[57] Morozov, Y.D., Simbukhov, I.A., Dyakonov, D.L. (2012). Study of microstructure and properties of ultrahigh-strength pipe steel of strength category x120 prepared under laboratory conditions, Metallurgist, 56(7), pp. 510-518.
[58] Garcia, C.I., Hua, M.J., Liang, X., Suikannen, P., DeArdo, A.J. (2012).On the microstructure of plate steels for API-5L X120 applications. Materials Science Forum, vol. 706, Trans Tech Publ, pp. 17-23.
[59] Garcia, C.I. (2017).High strength low alloyed (HSLA) steels. Automotive Steels, Elsevier, pp. 145-167.
[60] Bannenberg, N., Streißelberger, A., Schwinn, V. (2007). New steel plates for the oil and gas industry, Steel Res. Int., 78(3), pp. 185-188.
[61] Contreras, A., López, A., Gutiérrez, E.J., Fernández, B., Salinas, A., Deaquino, R., Bedolla, A., Saldaña, R., Reyes, I., Aguilar, J. (2020). An approach for the design of multiphase advanced high-strength steels based on the behavior of CCT diagrams simulated from the intercritical temperature range, Mater. Sci. Eng. A, 772, pp. 138708.
[62] Lan, H.F., Du, L.X., Li, Q., Qiu, C.L., Li, J.P., Misra, R.D.K. (2017). Improvement of strength-toughness combination in austempered low carbon bainitic steel: The key role of refining prior austenite grain size, J. Alloys Compd., 710, pp. 702-710.
[63] Entezari, E., Avishan, B., Mousalou, H., Yazdani, S. (2018). Effect of Electro Slag Remelting (ESR) on the microstructure and mechanical properties of low carbon bainitic steel, Kov. Mater, 56, pp. 253-263.
[64] Wu, Q., Zikry, M.A. (2015). Dynamic fracture predictions of microstructural mechanisms and characteristics in martensitic steels, Eng. Fract. Mech., 145, pp. 54-66.
[65] Kim, S., Kwon, J., Kim, Y., Jang, W., Lee, S., Choi, J. (2013). Factors influencing fatigue crack propagation behavior of austenitic steels, Met. Mater. Int., 19(4), pp. 683-690.
[66] Sami, Z., Tahar, S., Mohamed, H. (2014). Microstructure and Charpy impact properties of ferrite–martensite dual phase API X70 linepipe steel, Mater. Sci. Eng. A, 598, pp. 338-342.
[67] Simm, T., Sun, L., McAdam, S., Hill, P., Rawson, M., Perkins, K. (2017). The influence of lath, block and prior austenite grain (PAG) size on the tensile, creep and fatigue properties of novel maraging steel, Materials (Basel)., 10(7), pp. 730.
[68] YM, K., NJ, K. (2002). Effect of microstructure on the yield ratio and low temperature toughness of linepipe steels, ISIJ Int., 42(12), pp. 1571-1577.
[69] Qi, X.Y., Du, L.X., Hu, J., Misra, R.D.K. (2018). High-cycle fatigue behavior of low-C medium-Mn high strength steel with austenite-martensite submicron-sized lath-like structure, Mater. Sci. Eng. A, 718, pp. 477-482.

[70] NACE International the Corrosion Society. (2015). NACE MR0175: Materials for use in H_2S-containing environments in oil and gas production.
[71] Hwang, Y.-I., Kim, H.-J., Song, S.-J., Lim, Z.S., Yoo, S.-W. (2017). Improving the ultrasonic imaging of hydrogen-induced cracking using focused ultrasound, J. Mech. Sci. Technol., 31(8), pp. 3803-3809.
[72] Findley, K.O., O'Brien, M.K., Nako, H. (2015). Critical Assessment 17: Mechanisms of hydrogen induced cracking in pipeline steels, Mater. Sci. Technol., 31(14), pp. 1673-1680.
[73] Dunne, D.P., Hejazi, D., Saleh, A.A., Haq, A.J., Calka, A., Pereloma, E. V. (2016). Investigation of the effect of electrolytic hydrogen charging of X70 steel: I. The effect of microstructure on hydrogen-induced cold cracking and blistering, Int. J. Hydrogen Energy, 41(28), pp. 12411-12423.
[74] Laureys, A., Pinson, M., Depover, T., Petrov, R., Verbeken, K. (2020). EBSD characterization of hydrogen induced blisters and internal cracks in TRIP-assisted steel, Mater. Charact., 159, pp. 110029.
[75] Li, J., Gao, X., Du, L., Liu, Z. (2017). Relationship between microstructure and hydrogen induced cracking behavior in a low alloy pipeline steel, J. Mater. Sci. Technol., 33(12), pp. 1504-1512.
[76] Park, J.H., Oh, M., Kim, S.J. (2017). Effect of bainite in microstructure on hydrogen diffusion and trapping behavior of ferritic steel used for sour service application, J. Mater. Res., 32(7), pp. 1295-1303.
[77] Shahzad, M., Tayyaba, Q., Manzoor, T., ud-din, R., Subhani, T., Qureshi, A.H. (2018). The effects of martensite morphology on mechanical properties, corrosion behavior and hydrogen assisted cracking in A516 grade steel, Mater. Res. Express, 5(1), pp. 16516, DOI: 10.1088/2053-1591/aaa55f.
[78] Ohaeri, E., Omale, J., Rahman, K.M.M., Szpunar, J. (2020). Effect of post-processing annealing treatments on microstructure development and hydrogen embrittlement in API 5L X70 pipeline steel, Mater. Charact., 161, pp. 110124, DOI: 10.1016/J.MATCHAR.2020.110124.
[79] Zhu, X., Li, W., Hsu, T.Y., Zhou, S., Wang, L., Jin, X. (2015). Improved resistance to hydrogen embrittlement in a high-strength steel by quenching-partitioning–tempering treatment, Scr. Mater., 97, pp. 21-24, DOI: 10.1016/J.SCRIPTAMAT.2014.10.030.
[80] Liu, Z.Y., Wang, X.Z., Du, C.W., Li, J.K., Li, X.G. (2016). Effect of hydrogen-induced plasticity on the stress corrosion cracking of X70 pipeline steel in simulated soil environments, Mater. Sci. Eng. A, 658, pp. 348-354.
[81] Xue, H.B., Cheng, Y.F. (2011). Characterization of inclusions of X80 pipeline steel and its correlation with hydrogen-induced cracking, Corros. Sci., 53(4), pp. 1201-1208.
[82] Rahman, K.M.M., Qin, W., Szpunar, J.A., Kozinski, J., Song, M., Zhu, N. (2021). New insight into the role of inclusions in hydrogen-induced degradation of fracture toughness: three-dimensional imaging and modeling, Philos. Mag., 101(8), pp. 976-996.
[83] Rahman, K.M.M., Mohtadi-Bonab, M.A., Ouellet, R., Szpunar, J., Zhu, N. (2019). Effect of electrochemical hydrogen charging on an API X70 pipeline steel with focus on characterization of inclusions, Int. J. Press. Vessel. Pip., 173, pp. 147-155.
[84] Miyoshi, E., Tanaka, T., Terasaki, F., Ikeda, A. (1976). Hydrogen-induced cracking of steels under wet hydrogen sulfide environment.
[85] Qin, W., Szpunar, J.A. (2017). A general model for hydrogen trapping at the inclusion-matrix interface and its relation to crack initiation, Philos. Mag., 97(34), pp. 3296-3316.
[86] Domizzi, G., Anteri, G., Ovejero-Garcıa, J. (2001). Influence of sulphur content and inclusion distribution on the hydrogen induced blister cracking in pressure vessel and pipeline steels, Corros. Sci., 43(2), pp. 325-339.
[87] Beidokhti, B., Dolati, A., Koukabi, A.H. (2009). Effects of alloying elements and microstructure on the susceptibility of the welded HSLA steel to hydrogen-induced cracking and sulfide stress cracking, Mater. Sci. Eng. A, 507(1-2), pp. 167-173.
[88] Liou, H.-Y., Shieh, R.-I., Wei, F.-I., Wang, S.-C. (1993). Roles of microalloying elements in hydrogen induced cracking resistant property of HSLA steels, Corrosion, 49(05).
[89] Zhang, S., Fan, E., Wan, J., Liu, J., Huang, Y., Li, X. (2018). Effect of Nb on the hydrogen-induced cracking of high-strength low-alloy steel, Corros. Sci., 139, pp. 83-96.
[90] Li, L., Song, B., Cai, Z., Liu, Z., Cui, X. (2019). Effect of vanadium content on hydrogen diffusion behaviors and hydrogen induced ductility loss of X80 pipeline steel, Mater. Sci. Eng. A, 742, pp. 712-721.
[91] Baba, K., Mizuno, D., Yasuda, K., Nakamichi, H., Ishikawa, N. (2016). Effect of Cu addition in pipeline steels on prevention of hydrogen permeation in mildly sour environments, Corrosion, 72(9), pp. 1107-1115.
[92] Mohtadi-Bonab, M.A. (2019). Effects of different parameters on initiation and propagation of stress corrosion cracks in pipeline steels: a review, Metals (Basel)., 9(5), pp. 590.
[93] Lynch, S.P. (2003). Mechanisms of hydrogen assisted cracking-a review, Hydrog. Eff. Mater. Behav. Corros. Deform.

Interact., pp. 449-466.
[94] Traidia, A., Alfano, M., Lubineau, G., Duval, S., Sherik, A. (2012). An effective finite element model for the prediction of hydrogen induced cracking in steel pipelines, Int. J. Hydrogen Energy, 37(21), pp. 16214-16230.
[95] Kittel, J., Ropital, F., Pellier, J. (2008). Effect of membrane thickness on hydrogen permeation in steels during wet hydrogen sulfide exposure, Corrosion, 64(10), pp. 788-799.
[96] Kharin, V., Toribio, J. (2005).Effect of residual stress profile on hydrogen embrittlement susceptibility of prestressing steel. Anales de Mecánica de la Fractura, vol. 22, Citeseer, pp. 464-469.
[97] Jack, T.A., Pourazizi, R., Ohaeri, E., Szpunar, J., Zhang, J., Qu, J. (2020). Investigation of the hydrogen induced cracking behaviour of API 5L X65 pipeline steel, Int. J. Hydrogen Energy, 45(35), pp. 17671-17684.
[98] Javadi, Y., Sweeney, N.E., Mohseni, E., MacLeod, C.N., Lines, D., Vasilev, M., Qiu, Z., Mineo, C., Pierce, S.G., Gachagan, A. (2021). Investigating the effect of residual stress on hydrogen cracking in multi-pass robotic welding through process compatible non-destructive testing, J. Manuf. Process., 63, pp. 80-87.
[99] Zapffe, C.A., Sims, C.E. (1941). Hydrogen embrittlement, internal stress and defects in steel, Trans. AIME, 145(1941), pp. 225-271.
[100] Oriani, R.A. (1972). A mechanistic theory of hydrogen embrittlement of steels, Berichte Der Bunsengesellschaft Für Phys. Chemie, 76(8), pp. 848-857.
[101] Lynch, S. (2012). Hydrogen embrittlement phenomena and mechanisms, Corros. Rev., 30(3-4), pp. 105-123.
[102] Beachem, C.D. (1972). A new model for hydrogen-assisted cracking (hydrogen "embrittlement"), Metall. Mater. Trans. B, 3(2), pp. 441-455.
[103] Robertson, I.M., Sofronis, P., Nagao, A., Martin, M.L., Wang, S., Gross, D.W., Nygren, K.E. (2015). Hydrogen embrittlement understood, Metall. Mater. Trans. B, 46(3), pp. 1085-1103.
[104] Huang, C. (2020). Numerical Modeling of Hydrogen Embrittlement.
[105] Sofronis, P., Liang, Y., Aravas, N. (2001). Hydrogen induced shear localization of the plastic flow in metals and alloys, Eur. J. Mech., 20(6), pp. 857-872.
[106] Liang, Y., Sofronis, P., Aravas, N. (2003). On the effect of hydrogen on plastic instabilities in metals, Acta Mater., 51(9), pp. 2717-2730.
[107] Gerberich, W.W. (1974). Effect of hydrogen on high-strength and martensitic steels, Hydrog. Met., pp. 115-147.
[108] Gerberich, W.W., Chen, S. (1990).Environment-induced cracking of metals, fundamental processes: micromechanics. Proceedings of the First International Conference on Environment-Induced Cracking of Metals,(Houston, TX: NACE, 1989), pp. 167-187.
[109] González-Velázquez, J.L. (2020). A Practical Approach to Fracture Mechanics, Elsevier.
[110] Diniz, D., Silva, E., Carrasco, J., Barbosa, J., Silva, A. (2014). Effect of reversible hydrogen trapping on crack propagation in the API 5CT P110 Steel-a numerical simulation, Int. J. Multiphys., 8(3), pp. 313-324.
[111] McNabb, A., Foster, P.K. (1963). A new analysis of diffusion of hydrogen in iron and ferritic steels, Trans. Metall. Soc. AIME, 227(3), pp. 618.
[112] Balueva, A. (2014). Modeling of hydrogen embrittlement cracking in pipelines under high pressures, Procedia Mater. Sci., 3, pp. 1310-1315.
[113] Traidia, A., El-Sherik, A.M., Duval, S., Lubineau, G., El-Yagoubi, J. (2014). Model of parameters controlling resistance of pipeline steels to hydrogen-induced cracking, Corrosion, 70(1), pp. 87-94.
[114] Gonzalez JL, Rivas D, Dorantes H, Vazquez P, G.W. (2015).Modeling and simulation of cracked area growth rate of hydrogen-induced cracking in pipeline steels. 10th international symposium on advanced science and technology in experimental mechanics-Japan.
[115] Brouwer, R.C., de Mul, L.M., van den Handel, G. (1995). Modelling hydrogen induced crack growth: validation by comparison with experiment, NACE International, Houston, TX (United States).
[116] Hara, T., Asahi, H., Ogawa, H. (2004). Conditions of Hydrogen-Induced Corrosion Occurrence of X65 Grade Line Pipe Steels in Sour Environments, December 2004, Corrosion, 60 (12).

NOMENCLATURE

A	Austenite
AcC	Accelerated Cooling
AIDE	Adsorption-Induced Dislocation Emission

CCT	Continuous Cooling Transformation
F	Ferrite
FRT	Finishing Rolling Temperature
FCT	Finishing Cooling Temperature
GB	Globular Bainite
HEDE	Hydrogen Enhanced Decohesion
HELP	Hydrogen-Enhanced- Localized Plasticity
HIC	Hydrogen- Induced Plasticity
HPT	Hydrogen Pressure Mechanism
HOP	Heat treatment Online Process
HSLA	High Strength Low Alloy Steel
M	Martensite
Ms	Martensite Start Temperature
Mf	Martensite Finish Temperature
NMI	Non- Metallic Inclusions
P_{H2S}	Hydrogen Partial Pressure
SSC	Stress Sulfide Corrosion
SOHIC	Stress-Orientated Hydrogen-Induced Cracking
TLM	Tempered Lath Martensite
TMCP	Thermomechanical Control Process
TTT	Time-Temperature-Transformation
T_{nR}	Non-Recrystallization Temperature
QPT	Quenching- Partitioning- Tempering
QT	Quenching and Tempering